Effects of volcanism on climate

Paul Withers – 2000.02.18

Dave Kring's volcanology class

USGS
USGS Photo by J.N. Marso, July 1991

Early volcanism-climate relations

- Etna, 44BC
- Laki, Iceland, 1783, and Franklin
- Tambora, Indonesia, 1815, Year without Summer, *Frankenstein*, and Turner's sunsets
- Krakatoa, Indonesia, 1883, lots of optical effects

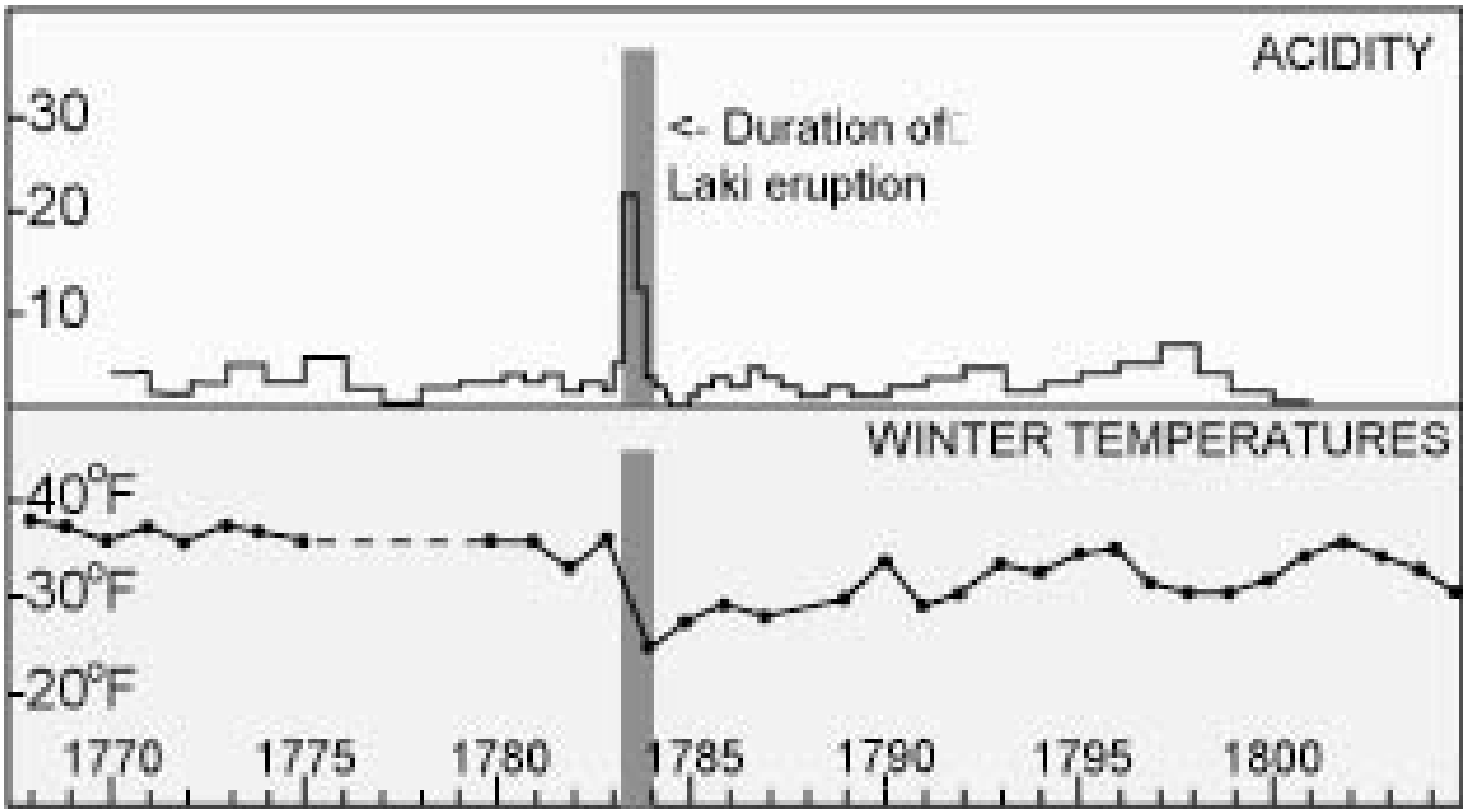
ACIDITY
-30
-20
-10
<- Duration of
Laki eruption
WINTER TEMPERATURES
-40°F
-30°F
-20°F
1770
1775
1780
1785
1790
1795
1800

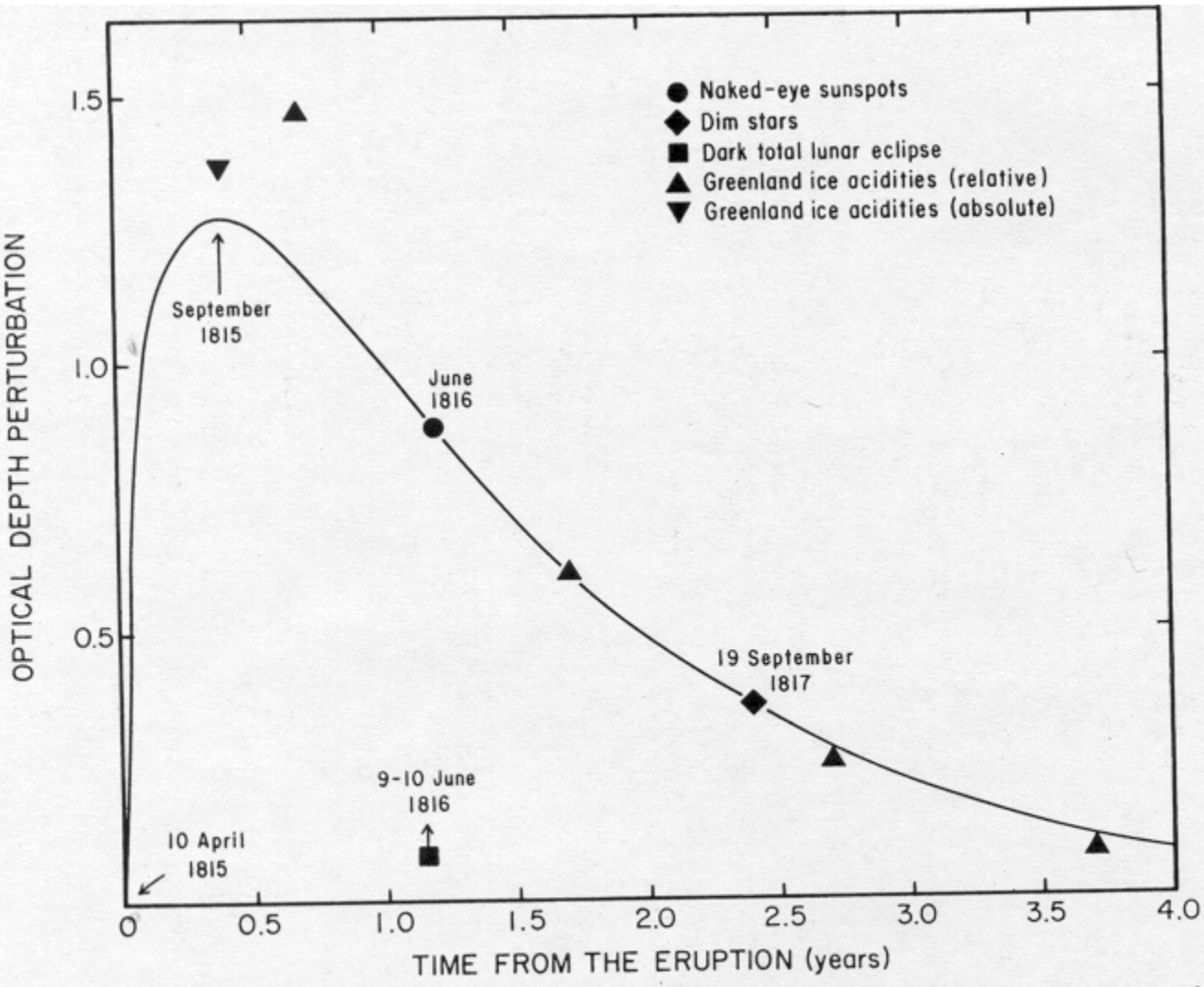

Figure 2 Excess visual optical depth at northern latitudes as a function of time reckoned from the date of the 1815 Tambora eruption. The plotted point for 9–10 June 1816 is only the lower limit to the true value (after Stothers 1984a).

Contents of volcanic plumes

- Ash, irrelevant (cf Kuwait)
- Gases – 80% H_2O, 10% CO_2, 5% SO_2, traces of halogens
- Entrained air

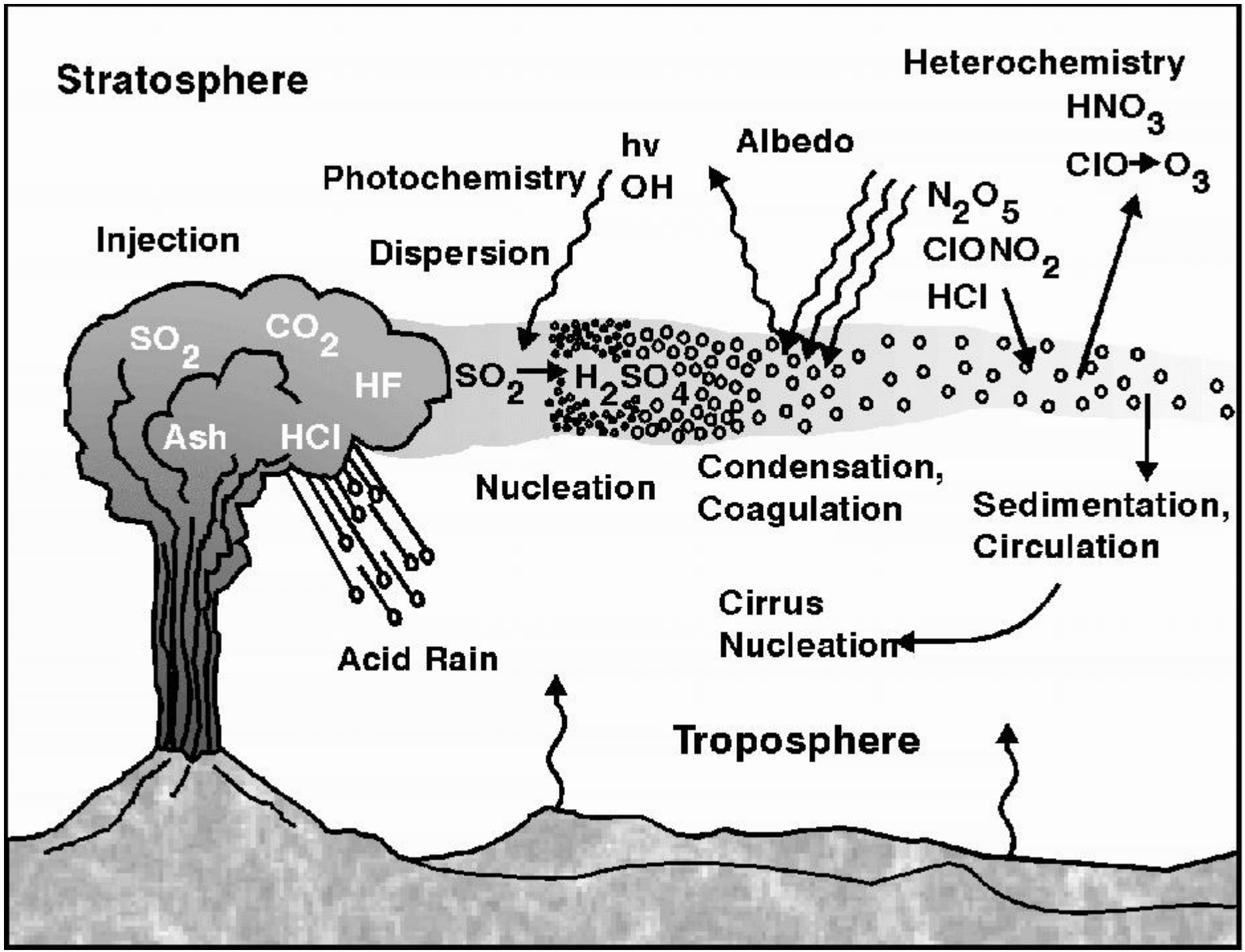
Stratosphere
Heterochemistry
HNO_3
hv
OH
Albedo
ClO → O_3
Photochemistry
N_2O_5
$ClONO_2$
HCl
Injection
Dispersion
SO_2
CO_2
HF
Ash
HCl
SO_2 → H_2SO_4
Nucleation
Condensation,
Coagulation
Sedimentation,
Circulation
Cirrus
Nucleation
Acid Rain
Troposphere

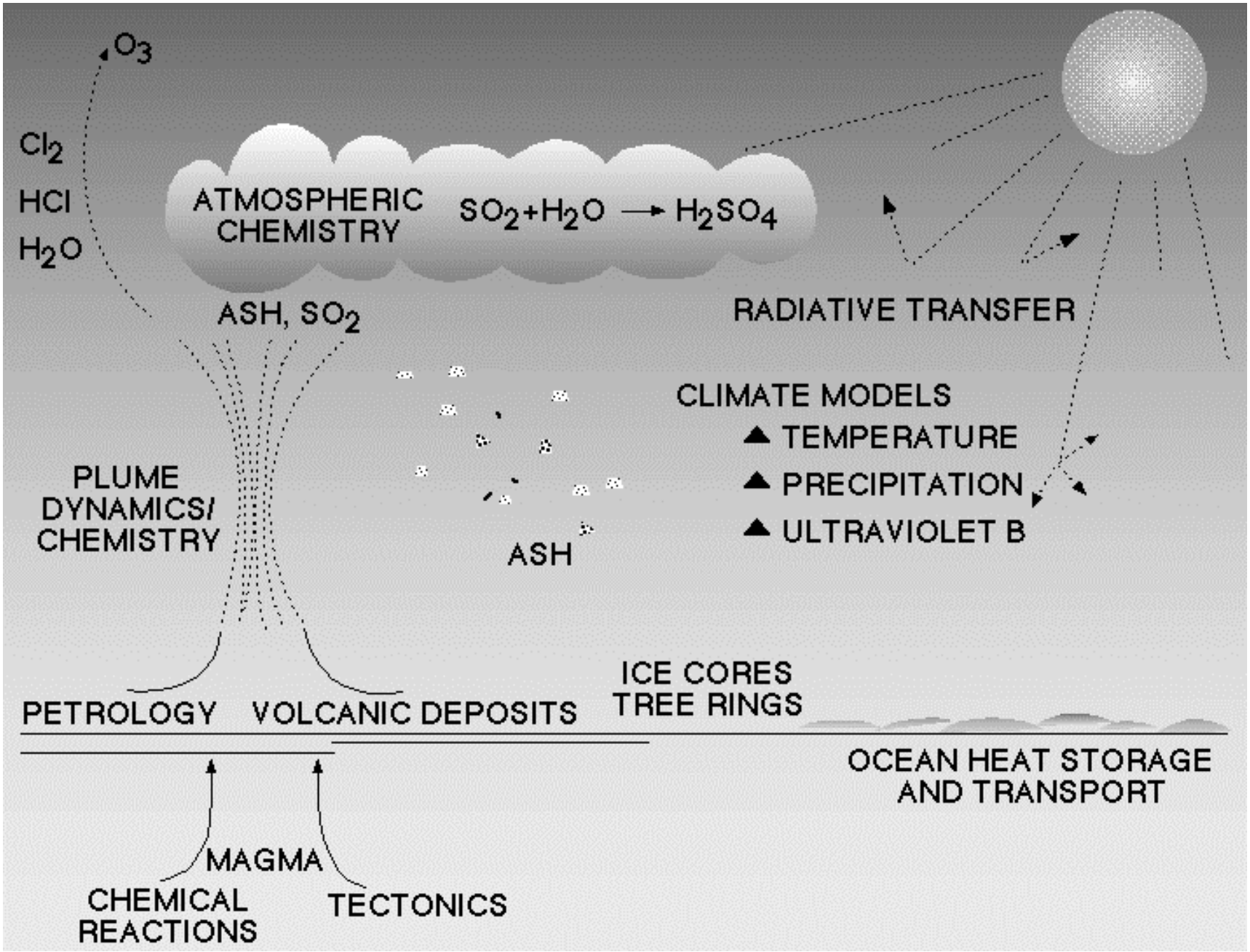
O_3
Cl_2
HCl
H_2O
ATMOSPHERIC CHEMISTRY
$SO_2+H_2O \rightarrow H_2SO_4$
ASH, SO_2
RADIATIVE TRANSFER
CLIMATE MODELS
TEMPERATURE
PRECIPITATION
ULTRAVIOLET B
PLUME DYNAMICS/ CHEMISTRY
ASH
ICE CORES
TREE RINGS
PETROLOGY
VOLCANIC DEPOSITS
OCEAN HEAT STORAGE AND TRANSPORT
MAGMA
CHEMICAL REACTIONS
TECTONICS

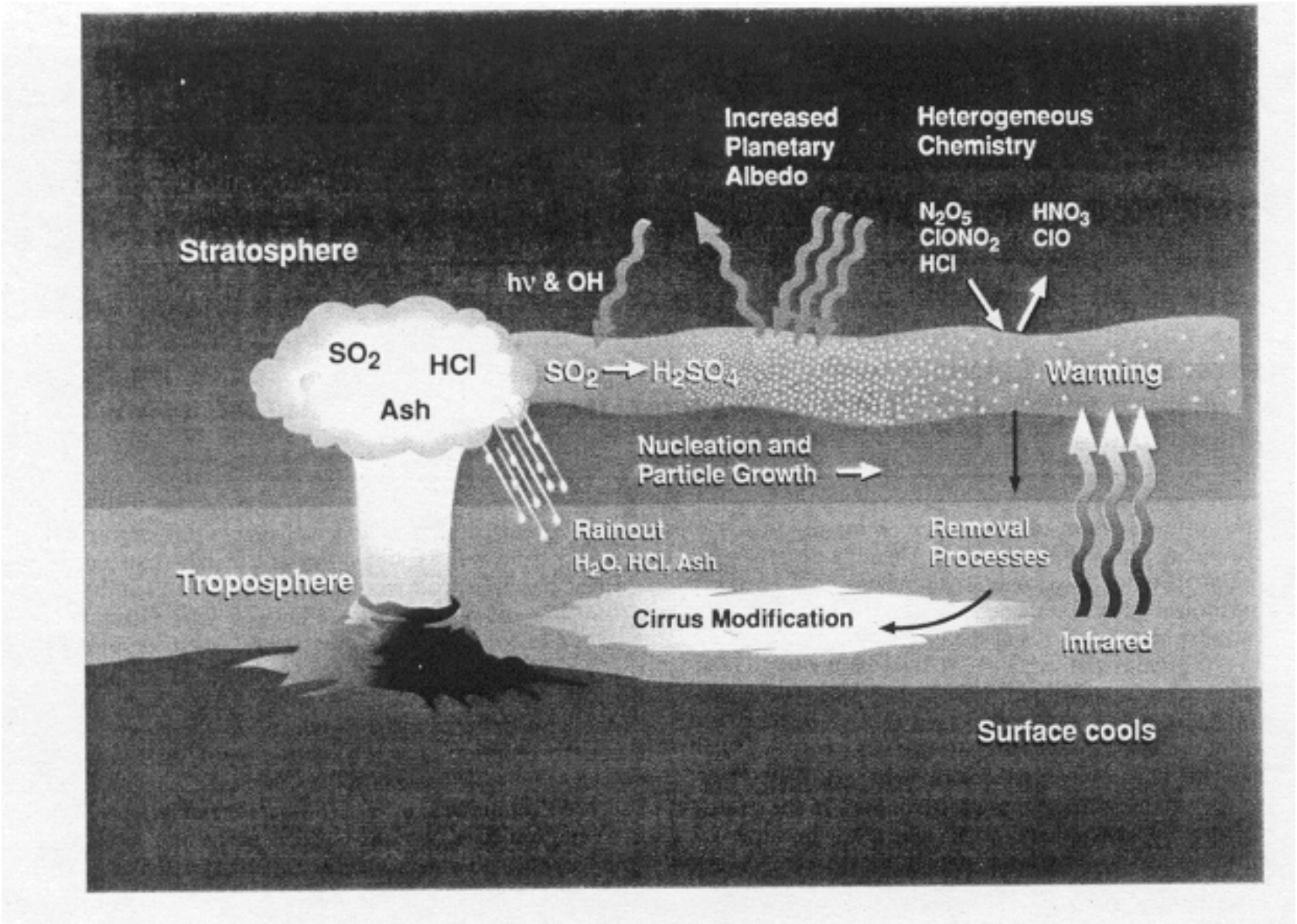
Increased
Planetary
Albedo
Heterogeneous
Chemistry
N_2O_5
$ClONO_2$
HCl
HNO_3
ClO
Stratosphere
hν & OH
SO_2
HCl
Ash
$SO_2 \rightarrow H_2SO_4$
Warming
Nucleation and
Particle Growth
Rainout
H_2O, HCl, Ash
Removal
Processes
Troposphere
Cirrus Modification
Infrared
Surface cools

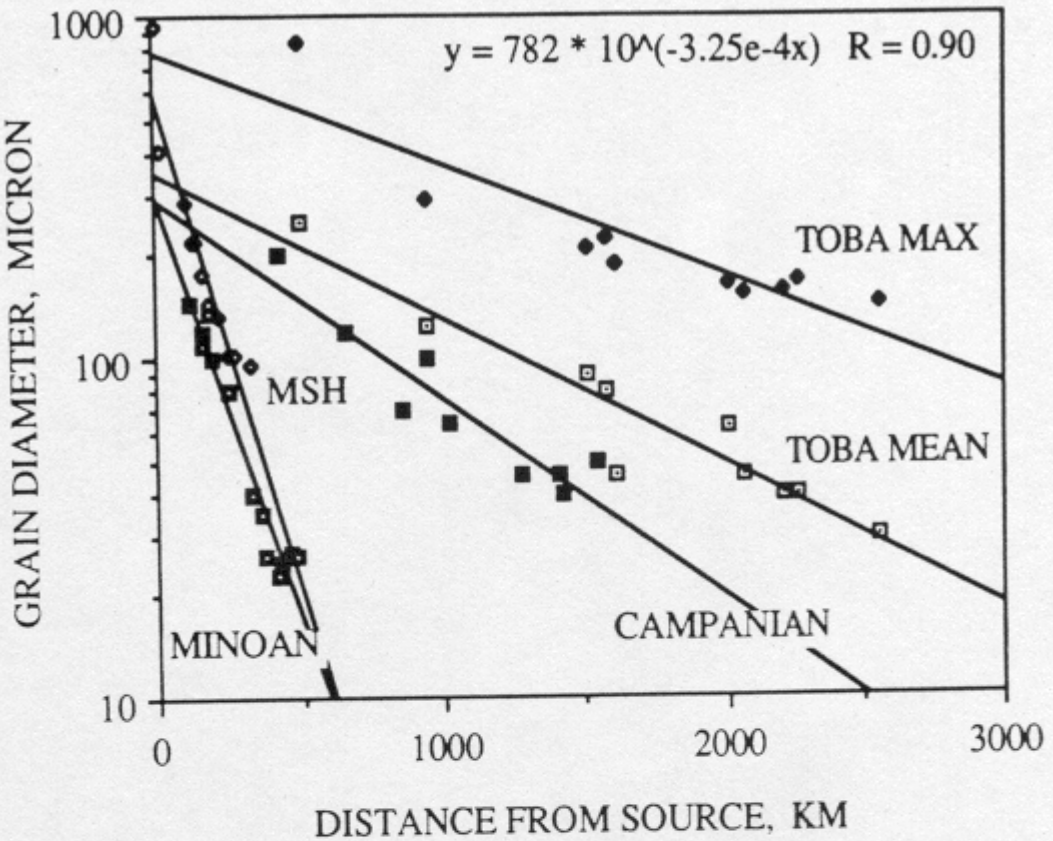

Figure 2. Atmospheric transport of tephra or volcanic ash from explosive volcanic eruptions. The diagram shows grain diameter (μm) versus distance along the down-wind axis (km). Note the much greater dispersal of tephra from eruptions during glacial stages, as compared to the two Holocene events. This may be attributed to increased atmospheric vigor during glacial stages, as column heights of, for example, the Campanian and Minoan Mediterranean volcanic events are similar. In case of the Toba eruption (75 ka), data is shown for the mean grain size and the maximum grain size observed down-wind (Ninkovich and others, 1978). The equation gives the exponential relation of grain size and distance for the maximum component of the Toba fallout. Data for the Campanian eruption in Italy (38 ka) show the grain size of the coarse mode of the bimodal deposit (Cornell and others, 1983). Data for the Minoan (3,500 B.P.) and Mount St. Helens (1980) events are also for the coarse modes of the bimodal fallout (Sparks and Huang, 1980; Carey and Sigurdsson, 1982).

Sulphur

- 75% H_2SO_4 – 25% H_2O liquid aerosols, submicron size
- Injected into stratosphere with month-long residence times
- Interacts with radiation to give tropospheric cooling and stratospheric heating
- Surfaces provide reaction sites for chemistry

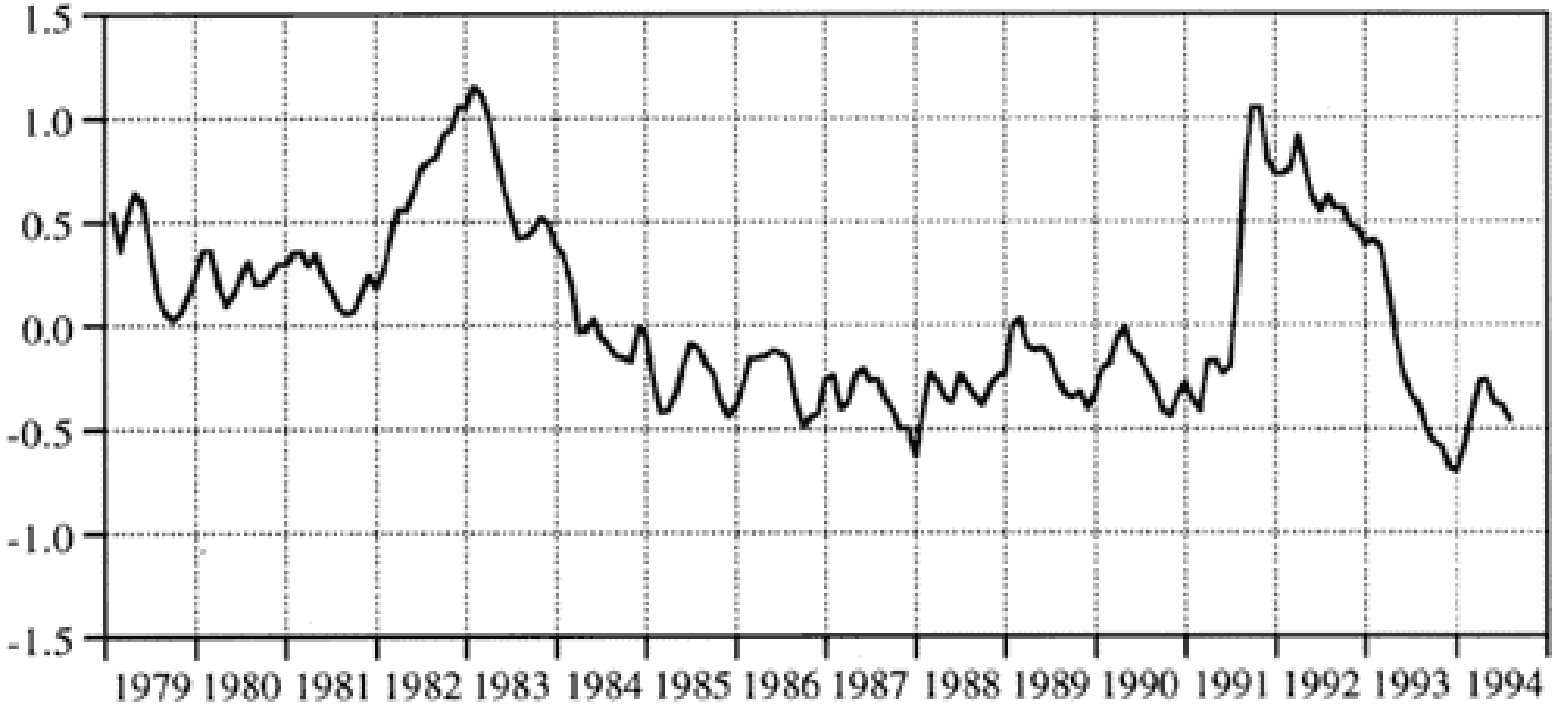

Lower stratosphere temperature anomalies,
85S-85N, 1982-1991 base period

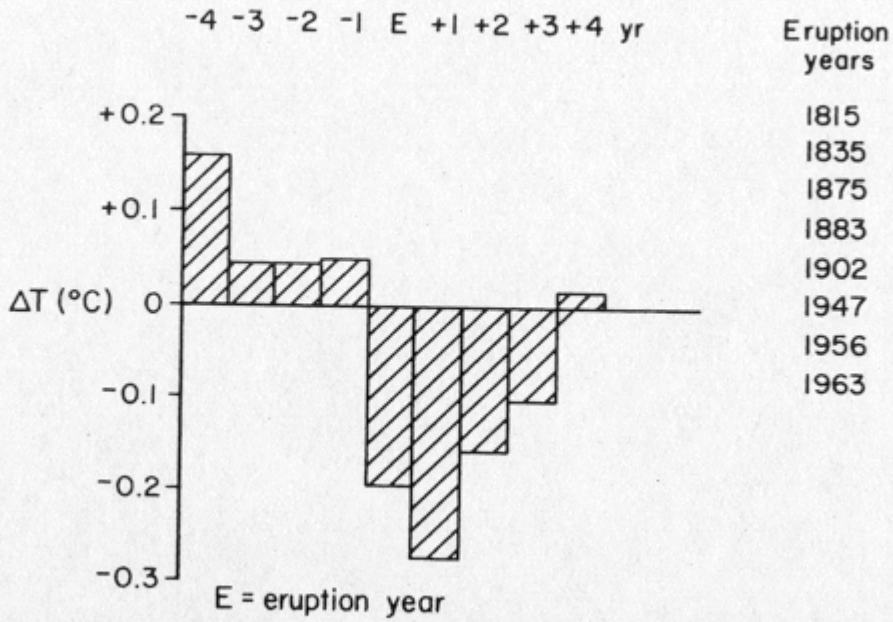

Figure 1 Composite plot of the temperature departure for the Northern Hemisphere in the four years immediately before and after some large nineteenth and twentieth century eruptions (after Self et al 1981).

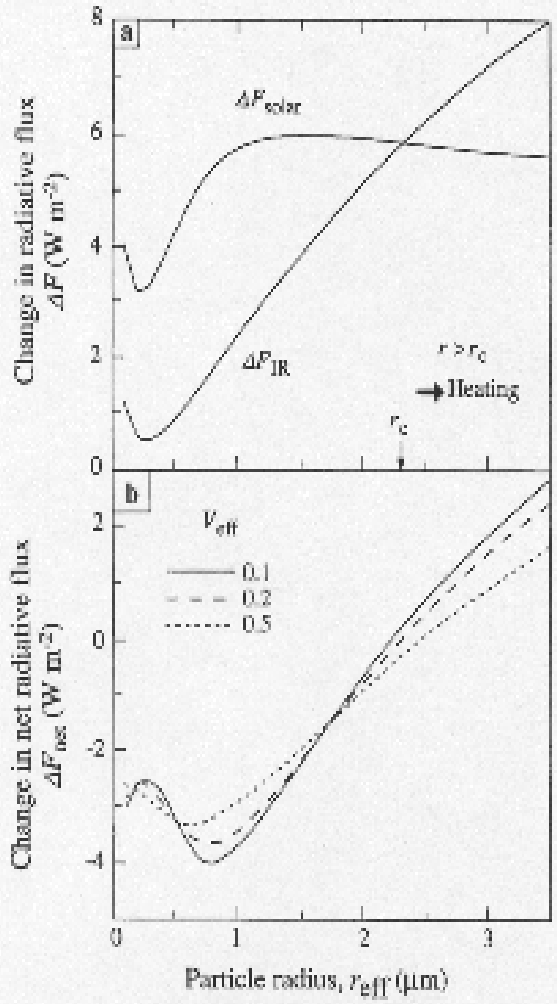

Figure 18.2 Theoretical models of climate forcing by a stratospheric aerosol layer (after Lacis *et al.* 1992). (a) Shows the change of solar flux, ΔF_{solar} (cooling), and infrared thermal flux, ΔF_{IR} (warming), at the tropopause, as a function of aerosol radius, caused by adding a stratospheric aerosol layer at 20–25 km altitude, with an optical depth $\tau = 0.1$. (b) Shows the change of the net radiative flux, ΔF_{net} at the tropopause for an aerosol optical depth $\tau = 0.1$, as a function of aerosol radius, and for three values of effective variance or width of the particle size distribution, V_{eff}. Multiplying ΔF_{net} by 0.3 yields ΔT (°C), the equilibrium air temperature change at the Earth's surface

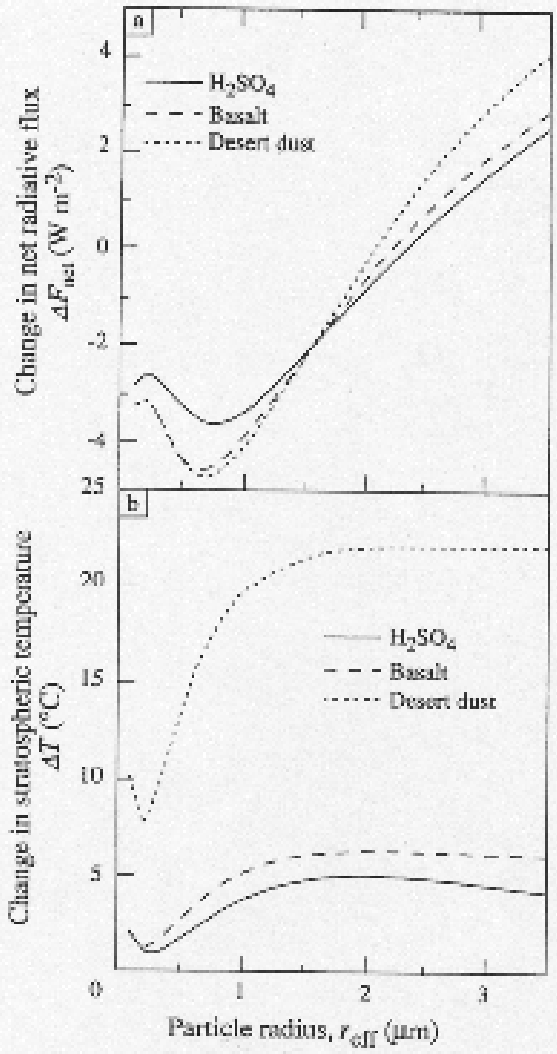

Figure 18.3 The effect of aerosol composition on (a) the net radiative flux, ΔF_{net}, in watts per square metre, and (b) the change in temperature in the stratospheric aerosol layer, as a function of effective aerosol radius, for optical depth $\tau = 0.1$ (after Lacis *et al.* 1992). Sulphuric acid is representative of a typical volcanic aerosol. A basalt dust layer is representative of the optical properties of glassy particles from most explosive volcanic eruptions. The large differences in the temperature change of an aerosol layer with desert dust in (b) is due to its strong absorption of solar radiation (a large real refractive index)

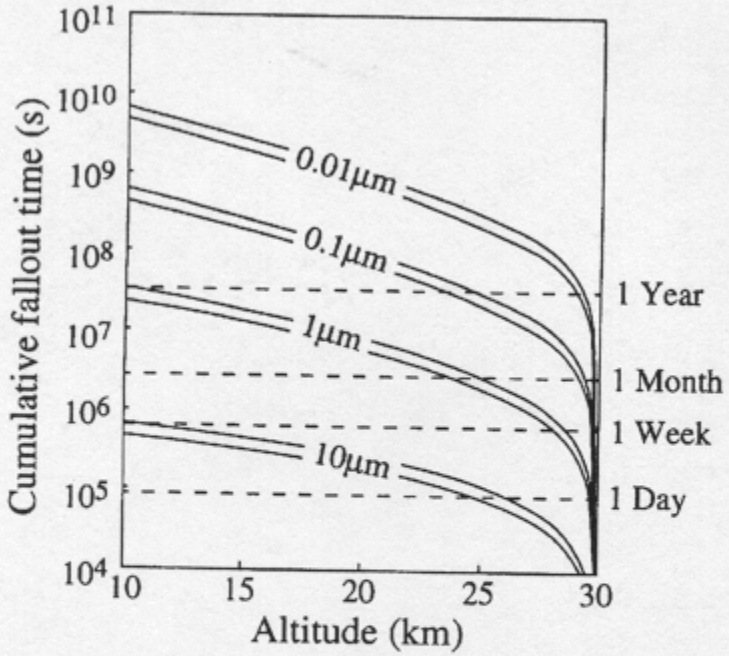

Figure 18.6 The cumulative fallout time (seconds) for sulphuric acid aerosols (the upper of each pair of curves) and volcanic glass particles, in the range 0.01, 0.1, 1 and 10 μm radius, as a function of altitude in the stratosphere, down to the tropopause (*c.* 10 km). These settling times are calculated for an initial aerosol injection at 30 km altitude, from the data of Kasten (1968) for a 1962 US standard atmosphere

Important factors

- Eruption volume
- Magma sulphur content (1 ppm to 1 wt%, more mafic, more sulphur)
- Eruption style (injection into stratosphere)
- Volcano location (global wind patterns)
- Tdecrease = 6e-5 $(S/grams)^{1/3}$ roughly…

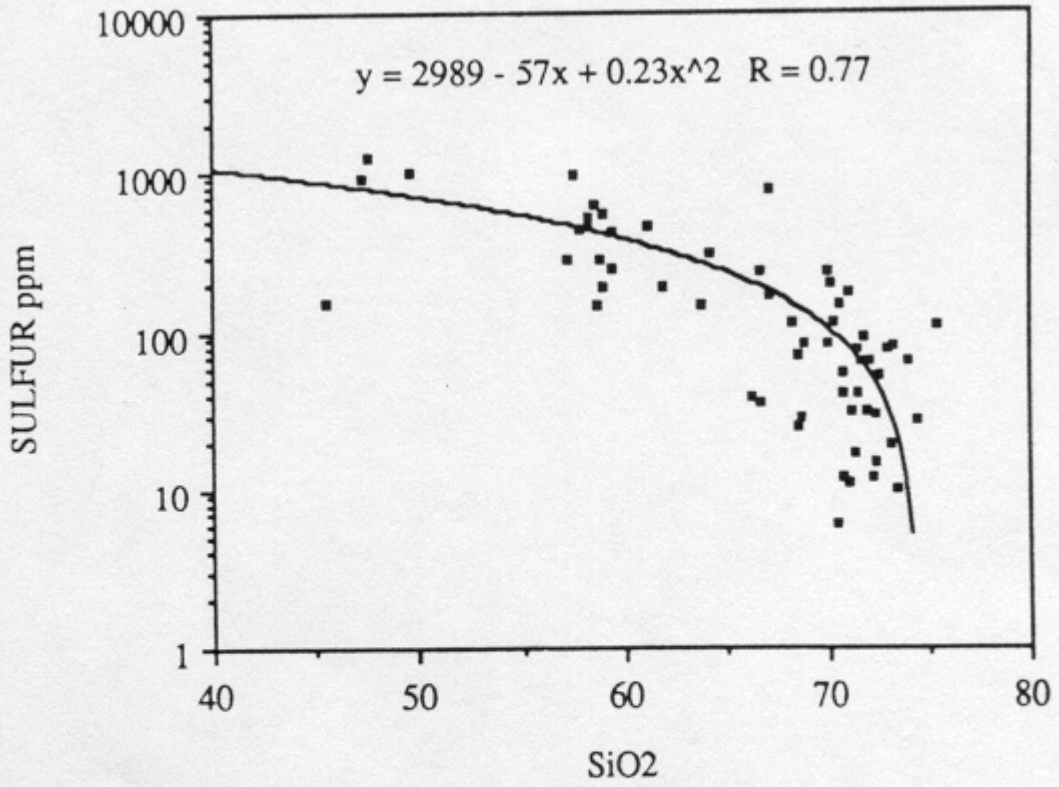

Figure 5. Yield of sulfur to the atmosphere (difference between glass inclusion concentration and sulfur concentration in degassed matrix glass) during volcanic eruptions, plotted as a function of SiO_2 content of the magma. Note the high sulfur yield during basaltic and trachyandesite eruptions, in contrast to the low yield for eruptions of rhyolite or other silicic magmas. Data from Palais and Sigurdsson (1989) and Devine and others (1984).

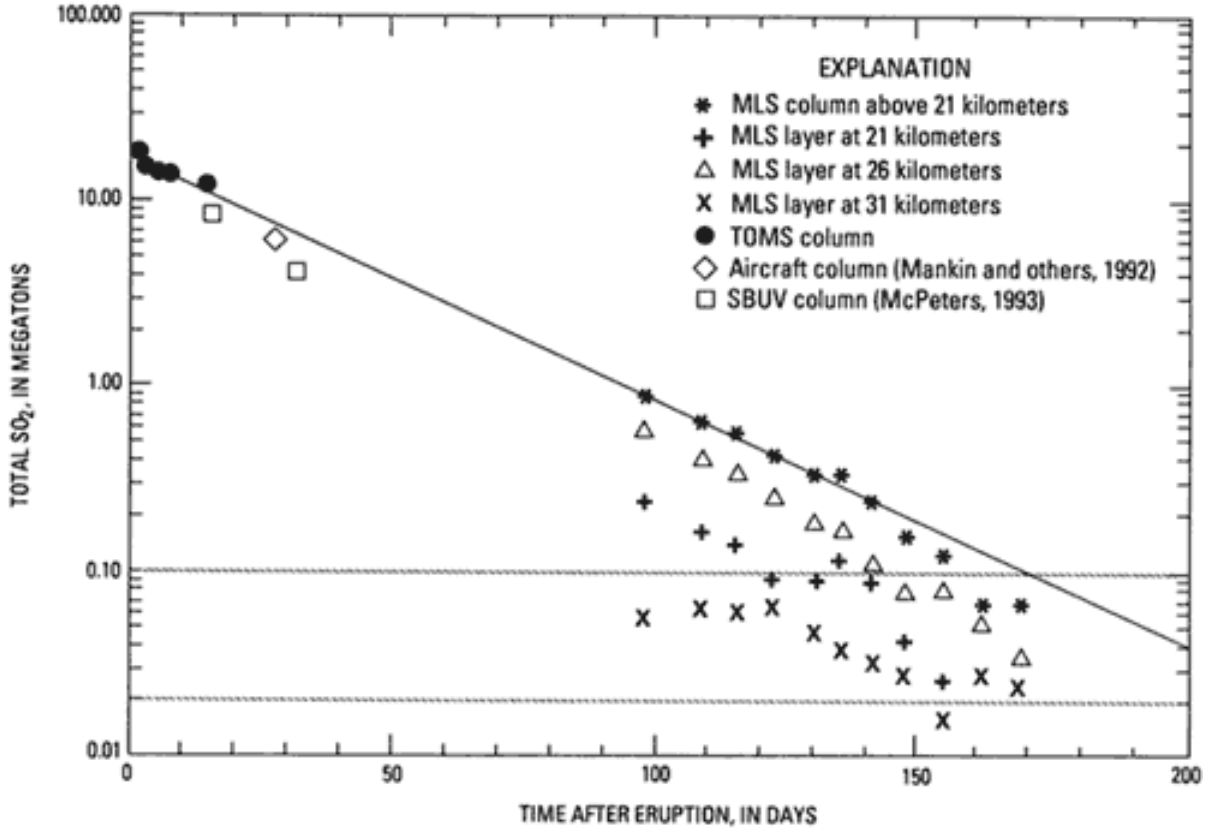

Measurements of the SO_2 produced by the June 15, 1991, Pinatubo eruption from MLS, TOMS, and SBUV determination between June 1991 and March 1993.

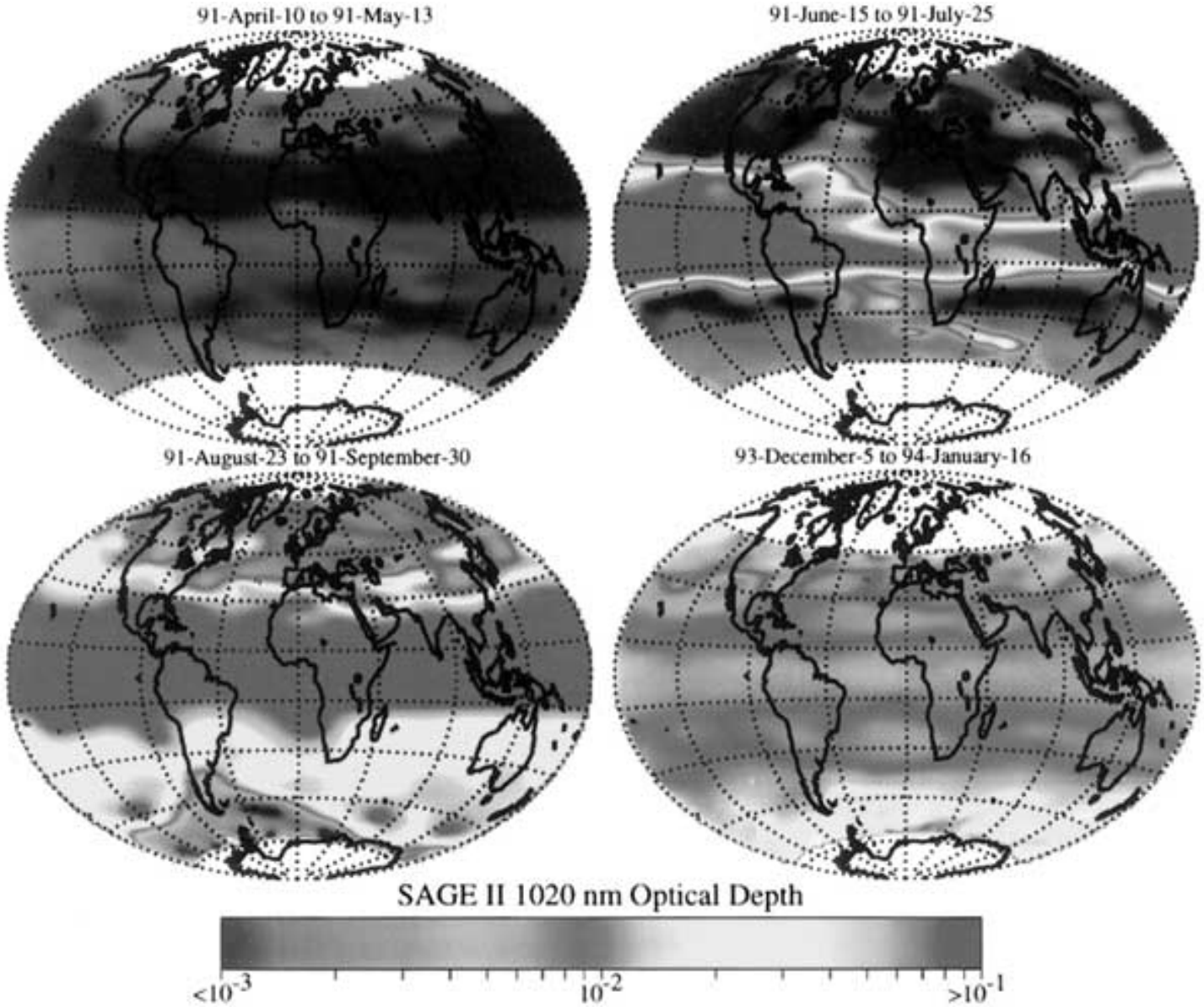
91-April-10 to 91-May-13
91-June-15 to 91-July-25
91-August-23 to 91-September-30
93-December-5 to 94-January-16
SAGE II 1020 nm Optical Depth
<10^-3
10^-2
>10^-1

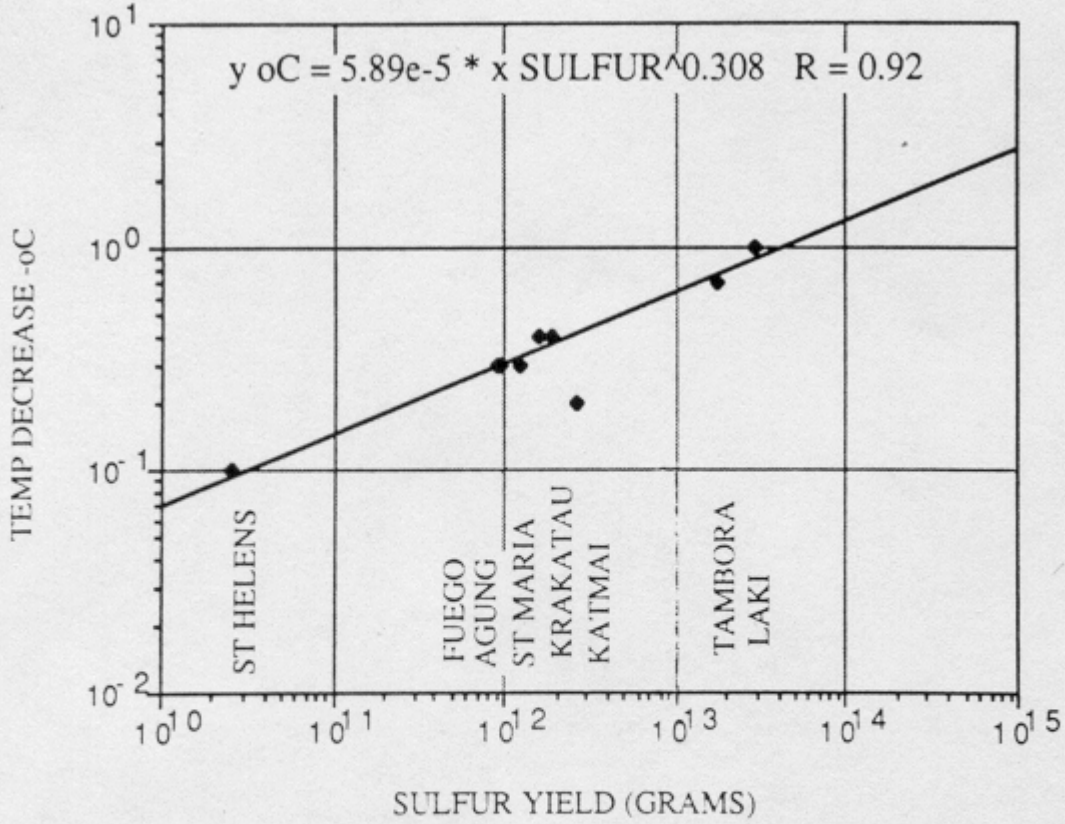

Figure 6. The observed relation between sulfur yield to the atmosphere during large volcanic eruptions and the Northern Hemisphere temperature decrease following the event. Sulfur-yield data from Sigurdsson (1982), Devine and others (1984), and Palais and Sigurdsson (1989). Climatological data from Rampino and Self (1982). The equation describes the best fit to the data, with a correlation coefficient of 0.92.

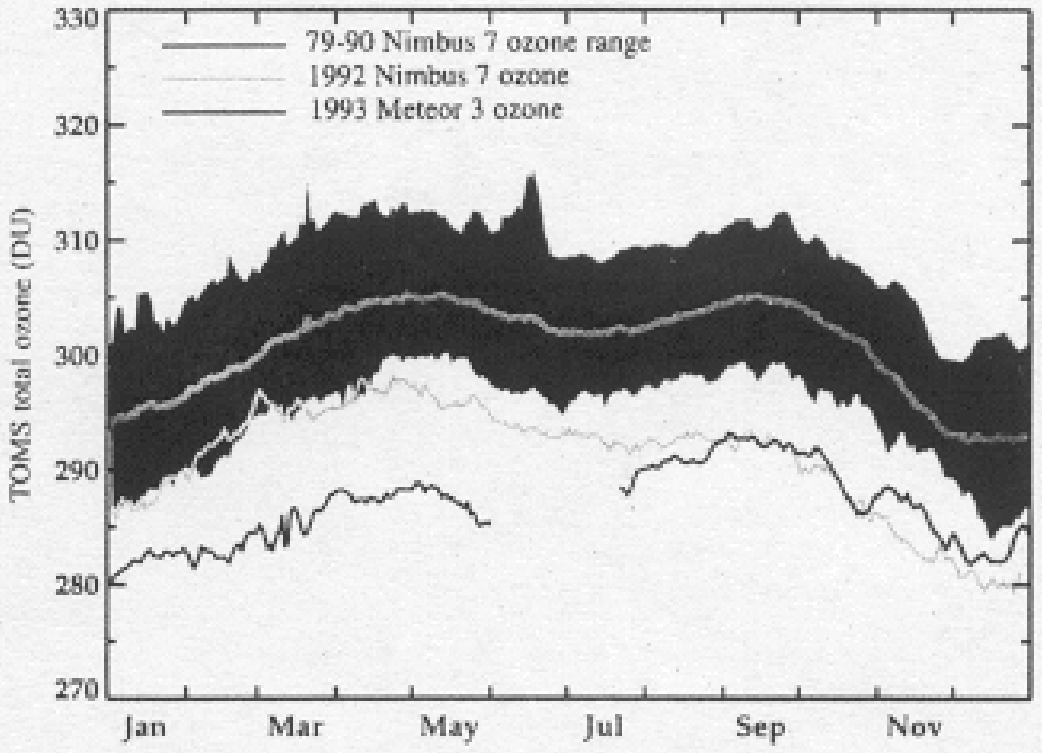

FIG. 4 Global mean ozone in Dobson units (DU) from the total ozone mapping spectrometer (TOMS) measurements as a function of time. Light green line, TOMS/NIMBUS 7 measurements for 1992; red line, TOMS/METEOR 3 measurements for 1993. These two lines are superimposed on the range of TOMS-observed global (65° N–65° S) mean ozone between 1979 and 1990 (dark blue line). The dark green line is the average total ozone for this period. TOMS data show a notable decrease in column ozone amounts beginning in early 1992 and persisting to the end of 1993. The loss reached as much as 6% of the column mean in April 1992[72,73].

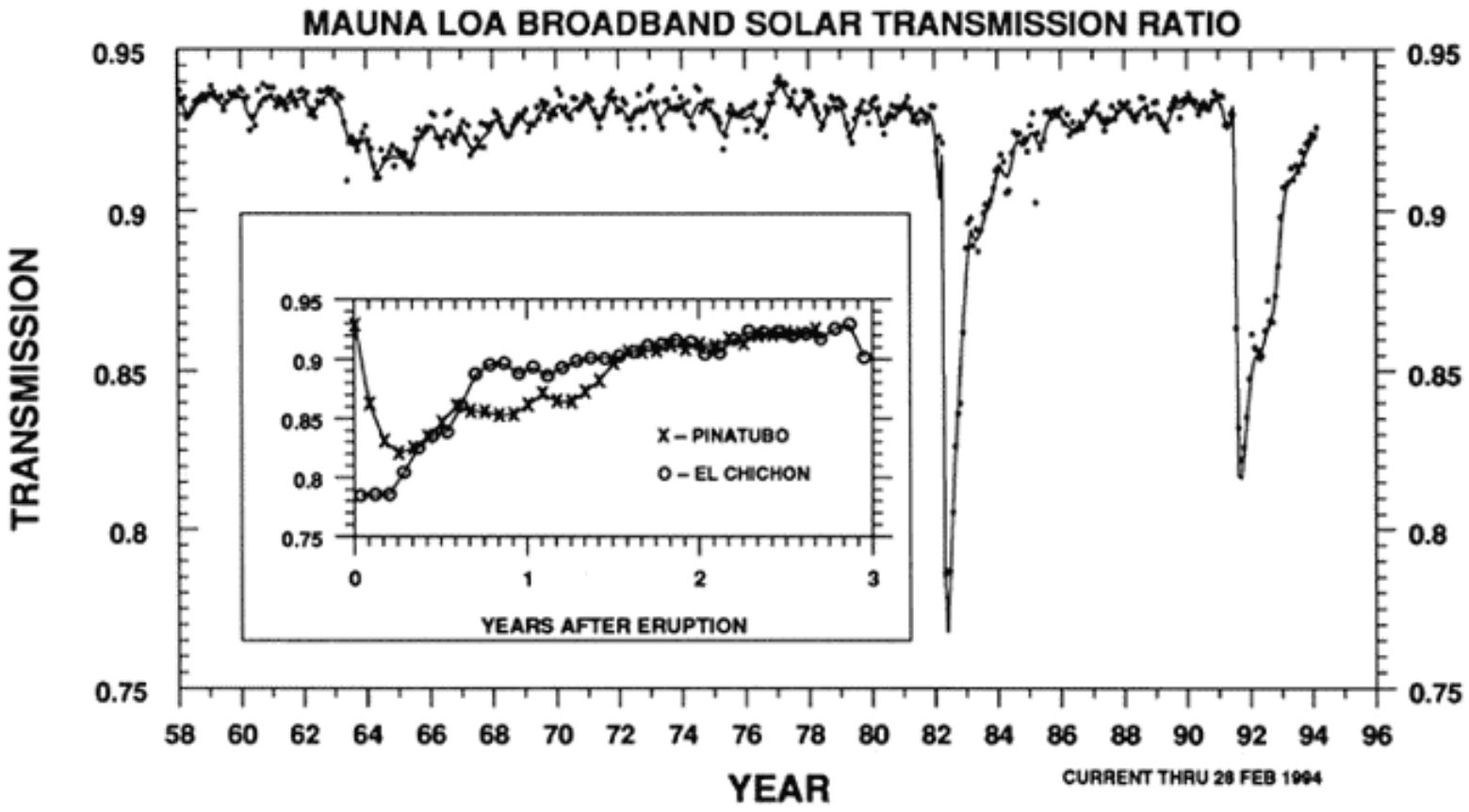
MAUNA LOA BROADBAND SOLAR TRANSMISSION RATIO
TRANSMISSION
0.95
0.9
0.85
0.8
0.75
58 60 62 64 66 68 70 72 74 76 78 80 82 84 86 88 90 92 94 96
YEAR
CURRENT THRU 28 FEB 1994
X – PINATUBO
O – EL CHICHON
0 1 2 3
YEARS AFTER ERUPTION

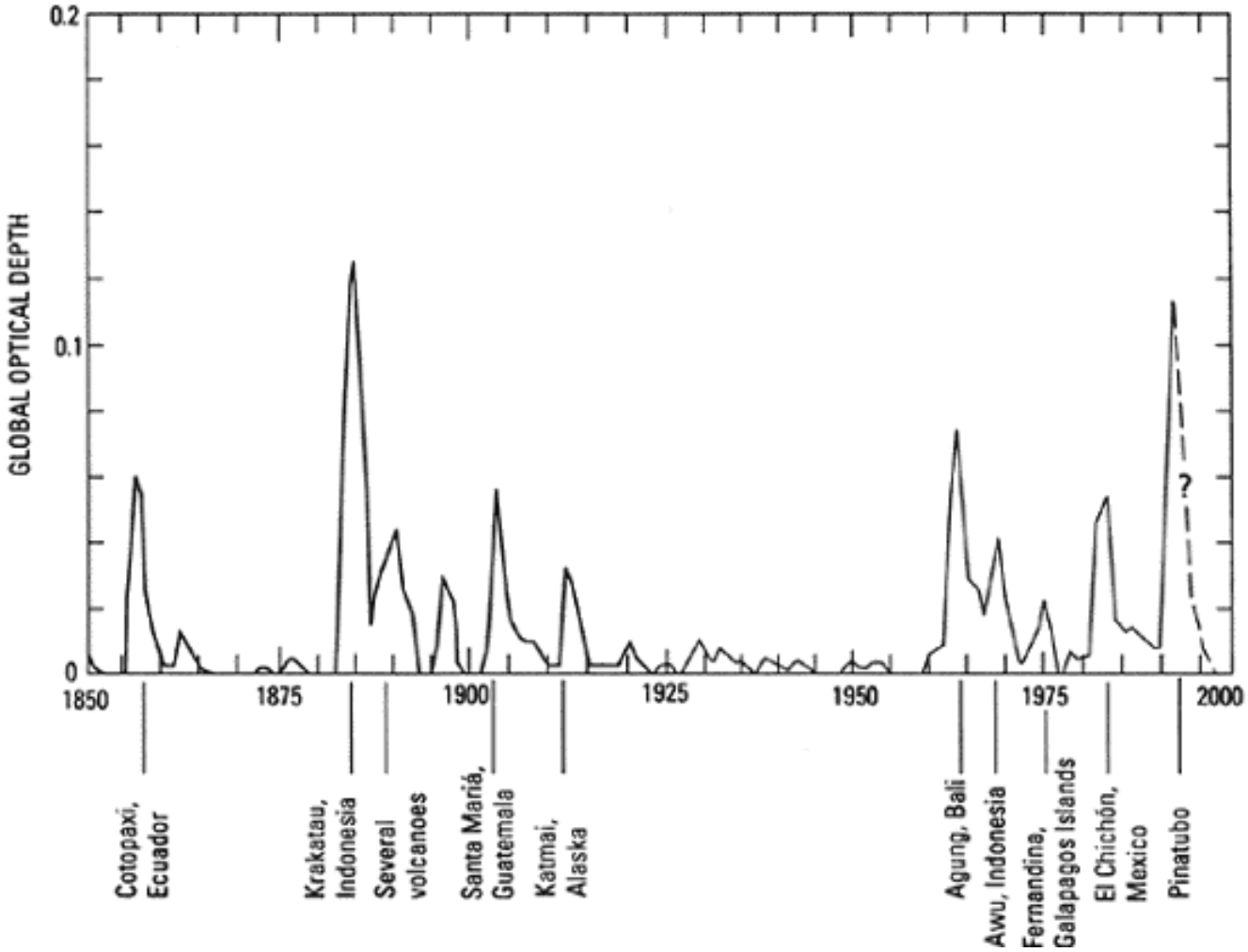
GLOBAL OPTICAL DEPTH
0.2
0.1
0
1850
1875
1900
1925
1950
1975
2000
?
Cotopaxi, Ecuador
Krakatau, Indonesia
Several volcanoes
Santa María, Guatemala
Katmai, Alaska
Agung, Bali
Awu, Indonesia
Fernandina, Galapagos Islands
El Chichón, Mexico
Pinatubo

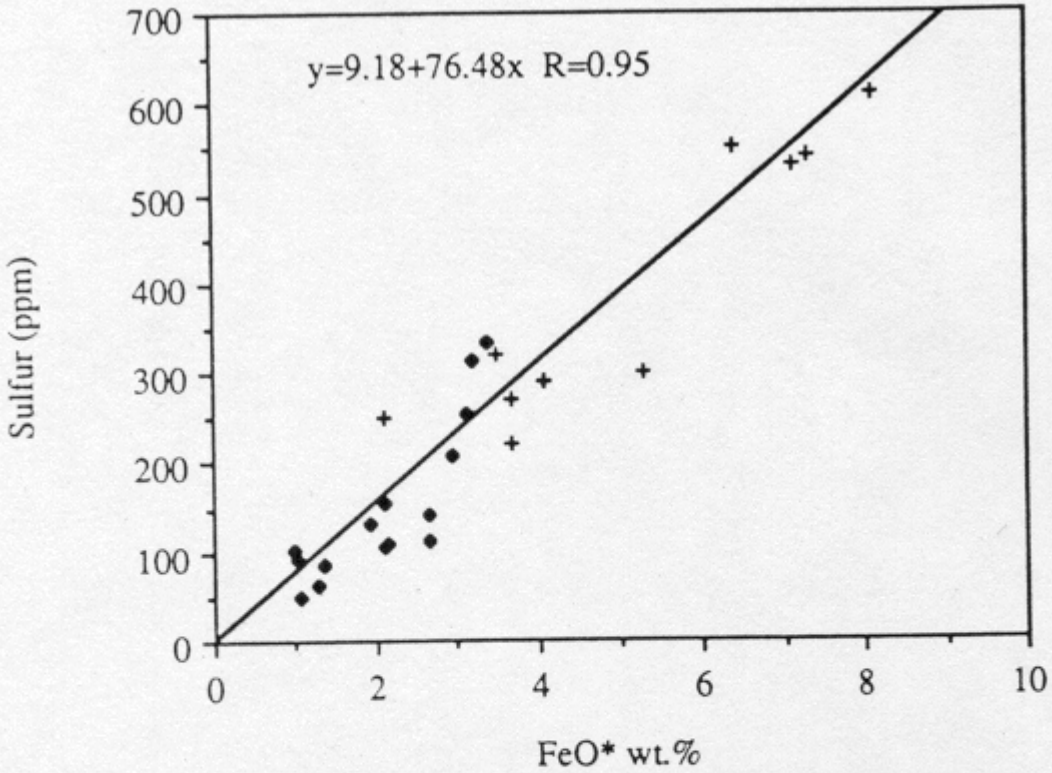

Figure 4. Sulfur solubility relations in silicic magmas, as a function of FeO^{total} content. Solid symbols show sulfur content in glass inclusions in phenocrysts from 1985 Nevada del Ruiz rhyodacite tephra (Sigurdsson and others, 1990). Crosses are results of hydrothermal experiments on sulfur solubility in Mount St. Helens 1980 dacite starting composition (after Carroll and Rutherford, 1985), at reduced oxygen fugacities (graphite-methane and quartz-magnetite-fayalite buffer curves) and 1 to 2 kbar, with $P_{total} = P_{fluid}$. The equation is a best-fit regression through the data, with a coefficient of correlation of 0.95.